In-depth insight into the electronic and steric effects of phosphine ligands on the mechanism of the R–R reductive elimination from $(PR_3)_2PdR_2$

Alireza Ariafard [a,b,*], Brian F. Yates [b,*]

[a] Department of Chemistry, Faculty of Science, Central Tehran Branch, Islamic Azad University, Shahrak Gharb, Tehran, Iran
[b] School of Chemistry, University of Tasmania, Private Bag 75, Hobart TAS 7001, Australia

ARTICLE INFO

ABSTRACT

The aim of this study was to investigate both the electronic and steric effects of the ancillary phosphine ligand L on the reductive elimination of Me–Me from a series of L_2PdMe_2 and $LPdMe_2$ complexes. Density functional theory was used to study these processes with the model ligands L = PMe_3, PH_3, PCl_3 and with the experimentally reported ligands L = PPh_3, PPh_2Me, $PPhMe_2$. For the model ligands we confirm that electron donation from L affects the barrier for reductive elimination from L_2PdMe_2 but not from $LPdMe_2$. In the former case the greater the electron donation or basicity of L, the greater the barrier and the later the transition state. This is because electron donation increases the σ^* antibonding between Pd and L in the transition structure. On the other hand, if L is a good π acceptor this stabilizes the occupied d_π orbital of Pd in the transition structure and lowers the barrier to reductive elimination. In the case of the reactions involving $LPdMe_2$ as the intermediate, it is the loss of the first L ($L_2PdMe_2 \rightarrow LPdMe_2 + L$) which determines the differences in the barrier height. Greater electron donation leads to greater L-to-Pd σ donation and a stronger Pd–L bond, and thus a greater overall barrier. A comparison of these results with the reductive elimination of 1,3-butadiene from divinyl palladium complexes L_2PdR_2 shows that the barriers are lower in the vinyl case because of a mix of orbital factors. Our results show that there is a significant stabilizing interaction between the Pd d_π orbital and the vinyl–vinyl hybrid σ^*/π^* orbitals in the reductive elimination transition structure. At the same time this Pd-R_2 orbital stabilization alleviates the potential antibonding interactions between Pd and L and makes the vinyl elimination much less susceptible to ancillary ligand effects. Energy-decomposition analyses have been used to elucidate the contributing factors to the activation energies for the reductive eliminations with the model phosphine ligands. These analyses have also been used to disentangle the electronic and steric effects involved in the larger ligand systems. The electronic effects of the experimentally reported ligands are found to be very similar to each other. On the other hand, steric effects lead to a destabilization of the reactant L_2PdMe_2 complexes but not the transition structures, which results in a decrease in the barriers to reductive elimination compared to the smaller phosphine ligands. These steric effects do not play a role in reductive elimination from $LPdMe_2$. These detailed analyses of the electronic and steric factors may be used to assist the design of systems which enhance or retard reductive elimination behaviour.

© 2009 Elsevier B.V. All rights reserved.

1. Introduction

Reductive elimination of R–R′ from $L_2Pd(R)(R')$, where L is typically a phosphine ligand, is a key bond-forming step in many cross coupling reactions catalyzed by palladium such as Stille and co-workers [1], Suzuki–Miyaura [2], Hiyama [3], Sonogashira [4], Kumada and co-workers [5], Negishi and Anastasia [6], and Heck [7]. Much work has already been done on the mechanism of this key step. Numerous studies have shown that reductive elimina-

tion, which reduces the oxidation state of palladium by two units, proceeds via a concerted mechanism involving a three-centered transition state (Scheme 1) [8]. The mechanism and rate of the reductive elimination reaction are mainly sensitive to the nature of the two reacting groups (R and R′) [9,10] and the steric and electronic properties of the ancillary ligand L [11].

During the course of the mechanistic studies of C–C bond-forming reactions, Yamamoto, Stille, and co-workers studied reductive elimination of saturated alkyl groups from cis-dialkylbis(phosphine)palladium complexes, $L_2Pd(R)(R')$, and found that the reaction would be preceded by the dissociation of one of the phosphine ligands to form a coordinatively unsaturated species $LPd(R)(R')$ adopting a T-shaped structure (Scheme 1) [9,12,13]. On the contrary, C–C couplings involving unsaturated vinyl and

* Corresponding authors. Address: Department of Chemistry, Faculty of Science, Central Tehran Branch, Azad University, Shahrak Gharb, Tehran, Iran (A. Ariafard).
E-mail addresses: ariafard@yahoo.com (A. Ariafard), Brian.Yates@utas.edu.au (B.F. Yates).

Concerted mechanism (direct reductive elimination)
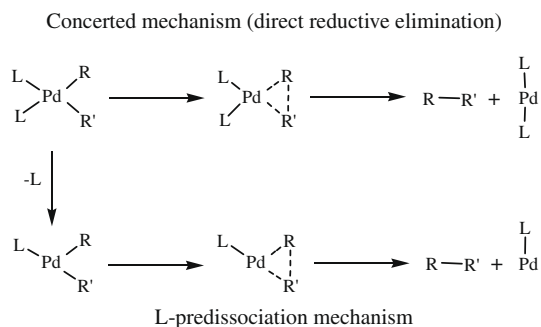
Scheme 1.

phenyl groups were found to be much faster and occur without prior phosphine dissociation [9]. There are numerous experimental studies in the literature on the reductive elimination of the unsaturated groups from square planar transition metal complexes [14,15]. From the experimental findings, Yamamoto and Stille suggested that the reductive elimination reaction proceeding directly from the four coordinate species should be much more difficult than that from the three coordinate species. This was supported by theoretical studies of Macgregor et al. [16]. In 2005, Musaev, Morokuma and co-workers reported DFT calculations on the ease of reductive elimination of R–R′ from $(PH_3)_2Pd(R)(R′)$ and concluded that, in agreement with the experimental data, the reductive elimination of two methyls is more difficult than the same process involving unsaturated groups [10].

The rate of reductive elimination is also reliant on the nature of the ancillary ligands L. The use of phosphine ligands with low electron-donating properties produces a clear enhancement in the rate of reductive elimination [11b]. The possible explanation for the trend is that Pd(II) complexes, which are more electrophilic than Pd(0) complexes, become more stable with phosphine ligands of high donicity [8e]. This feature stabilizes the initial complex $L_2Pd(R)(R′)$ with respect to the transition state, leading to an increase in the rate of reductive elimination. In addition, more bulky phosphines, acting as ancillary ligands, accelerate the reductive elimination process. For example, Negishi et al. studied the reductive elimination of R–R (R = Me, Ph, *t*-Bu-C≡C–, *t*-Bu-C≡C–) from a series of phosphine complexes of the type L_2PR_2, where L = PPh_3, PPh_2Me, and $PPhMe_2$, and concluded that the efficiency of the phosphines decreases in the following order $PPh_3 > PPh_2Me > PPhMe_2$ [11b]. Although the question of whether the above trend is mainly controlled by steric effects or electronic influences remain unanswered, the trend could be rationalized by the steric effect induced by the phosphine ligands; the larger the steric bulk, the easier the elimination [17]. Very recently, Ananikov et al. used a theoretical ONIOM study to investigate the R–R reductive elimination from L_2PdR_2 (L = PH_3, PMe_3, PPh_3, PCy_3) and found that steric parameters mainly influence the energy of the ground state while electronic parameters have the largest impact on the energy of the transition state [18].

Despite the extensive theoretical studies [11a,14,19], the reason why the three coordinate species $LPdR_2$ undergoes reductive elimination much more readily than the four coordinate species L_2PdR_2 has not been addressed clearly yet. In this contribution, we wish to provide a better understanding of how electronic properties of the ancillary ligand L affect the reductive elimination of Me–Me from both the model complexes L_2PdMe_2 and $LPdMe_2$, where L = PMe_3, PH_3, PCl_3, with the aid of B3LYP density functional theory (DFT) calculations. The representative set of L includes ligands with gradually changing donor and acceptor characters. The σ-donor character of L decreases as L = $PMe_3 > PH_3 > PCl_3$ while the π-acceptor character of L increases in the order L = $PMe_3 < PH_3 < PCl_3$ [20].

We also briefly investigate how the nature of R affects the preferred pathway. To elucidate the combined effects of the electronic and steric nature of L on the reductive elimination reaction, we also studied the Me–Me reductive elimination reaction from the real, experimentally reported, species Me_2PdL_2 and Me_2PdL, where L = PPh_3, PPh_2Me, and $PPhMe_2$. In this way, we will provide a consistent molecular orbital rationalization which encompasses 4-coordinate vs. 3-coordinate elimination, alkyl vs. vinyl elimination, and phosphine ligands with a range of electronic and steric effects.

2. Computational detail

GAUSSIAN 03 [21] was used to fully optimize all the structures reported in this paper at the B3LYP level of density functional theory [22]. The effective core potentials of Hay and Wadt with double-ζ valence basis sets (LanL2DZ) [23] were chosen to describe Pd, P and Cl. The 6-31G(d) basis set was used for other atoms [24]. Polarization functions were also added for $Cl(\zeta_d = 0.640)$ and $P(\zeta_d = 0.387)$ [25]. This basis set combination will be referred to as BS1. Frequency calculations were carried out at the same level of theory for structural optimization and confirmed that transition states have only one imaginary frequency. The natural bond orbital (NBO) program, as implemented in GAUSSIAN 03, was used to obtain natural populations of atoms [26].

To test the accuracy of the medium-size basis set (BS1) used, we carried out single point energy calculations for all structures (as well as full optimization of the structures given in Fig. 1) with a larger basis set: LANL2augmented:6-311+G(2d,p) basis set, incorpo-
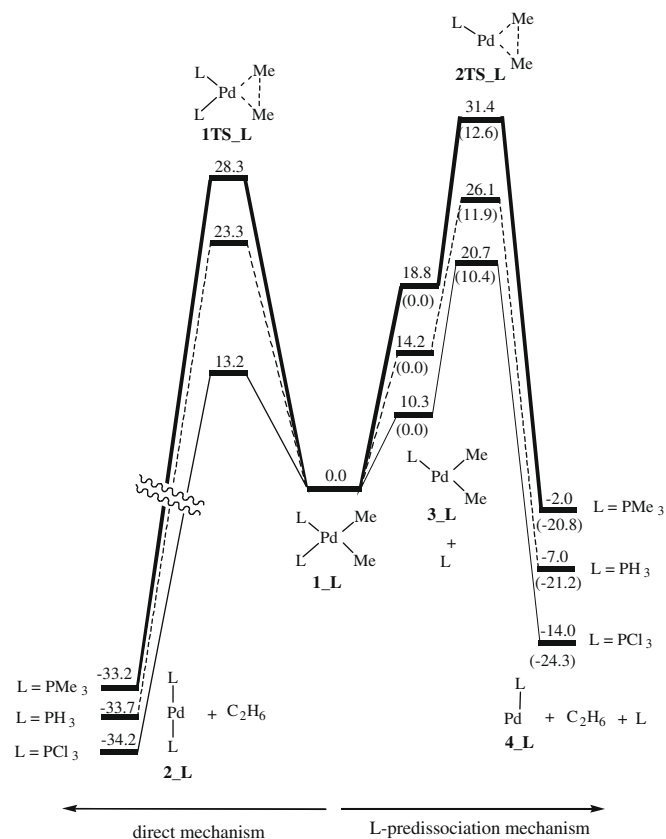

Fig. 1. Potential energy profiles calculated for the Me–Me reductive elimination from L_2PdMe_2 (L = PMe_3, PH_3, PCl_3) through both the direct and L-predissociation mechanisms using B3LYP/BS1. Values given in parentheses are relative to $3\_L + L$. The electronic energies relative to the L_2PdMe_2 are given in kcal/mol.

rating the LANL2 effective core potential, a large LANL2TZ+(3f) basis set on Pd (see Supplementary material), and the 6-311+G(2d,p) basis set on other atoms. This basis set will be referred to as BS2. The results show that basis set dependence is insignificant. For example, using the smaller basis set, the relative energies of **1TS_PPh₃**, **1TS_PPh₂Me**, and **1TS_PPhMe₂** (Fig. 6) are 20.4, 24.7, and 27.9 kcal/mol, respectively. Using the larger basis set, the relative energies are 20.8, 26.6, and 30.0 kcal/mol, respectively (for detailed information see Figs. S1–S4 in Supplementary material).

3. Results and discussion

3.1. Me–Me elimination from L_2PdMe_2 (L = PMe_3, PH_3, PCl_3)

Let us first discuss the effect of the electronic properties of L on the reductive elimination of ethane from L_2PdMe_2 (**1_L**) where L = PMe_3, PH_3, PCl_3. The calculated energy profiles using B3LYP/BS1 for the reductive elimination reaction on the basis of the two mechanisms summarized in Scheme 1 are shown in Fig. 1. It can be seen that the direct reductive elimination of ethane from L_2PdMe_2 for L = PCl_3, PH_3, and PMe_3 takes place with the activation barriers of 13.2, 23.3, and 28.3 kcal/mol, respectively. The overall activation barrier heights computed for the L-predissociation mechanism are 20.7, 26.1, and 31.4 kcal/mol for L = PCl_3, PH_3, and PMe_3, respectively. These results are consistent with the experimental observations that reductive elimination is accelerated by the presence of ancillary ligands with decreased electron-donating properties and increased electron-withdrawing properties. The exothermicity of the reaction of **1_L** → **2_L** is comparable for all the species and is not sensitive to the electronic nature of the ancillary ligand.

From Fig. 1, it is obvious that an increase in electron-donating properties of L has a significant effect on the energy of the transition state for the direct reductive elimination of ethane from the four coordinate species L_2PdMe_2, while it has a very little effect on the energy of the transition states for the reductive elimination from the three coordinate species $LPdMe_2$. The barrier to ethane elimination from L_2PdMe_2 spans a relatively large range from 13.2 kcal/mol (L = PCl_3) to 28.3 kcal/mol (L = PMe_3), while the barrier to ethane elimination from $LPdMe_2$ spans a relatively small range from 10.4 kcal/mol (L = PCl_3) to 12.6 kcal/mol (L = PMe_3). Therefore, for the L-predissociation mechanism, it is the L ligand loss step which contributes substantially to the differences in the overall barrier. The L dissociation energy in **1_PMe₃**, **1_PH₃**, and **1_PCl₃** is calculated as 18.8, 14.2, 10.3 kcal/mol, respectively, suggesting that dominating the bonding interaction between a Pd metal center and a L ligand is the L-to-Pd σ-donation.

It also follows from Fig. 1 that, for a given L, the barrier to ethane elimination from L_2PdMe_2 through the direct mechanism is favored over the L-predissociation mechanism. However, taking into account the entropic effect, ΔG could change this computational result. As expected, a large positive entropy change, ΔS, occurs in the L dissociation from L_2PdMe_2 because a one-to-two transformation occurs in the course of the reaction. The free energy change, ΔG, includes entropic contributions by taking into account the vibrational, rotational, and translational motions of the species under consideration. Our calculations in the gas phase overestimate the rotational and translational motions because these two motions are highly suppressed in solution [27]. This feature decreases noticeably ΔG as compared to ΔE. For example, the energy required for phosphine dissociation from $(PH_3)_2Pd(Me_3)_2$ is calculated as follows: ΔE = 14.2 kcal/mol and $ΔG_{298}$ = 0.6 kcal/mol. The energy difference between the ΔE and ΔG values (13.6 kcal/mol) is greater than the one suggested by Ziegler (8–10 kcal/mol) [28],
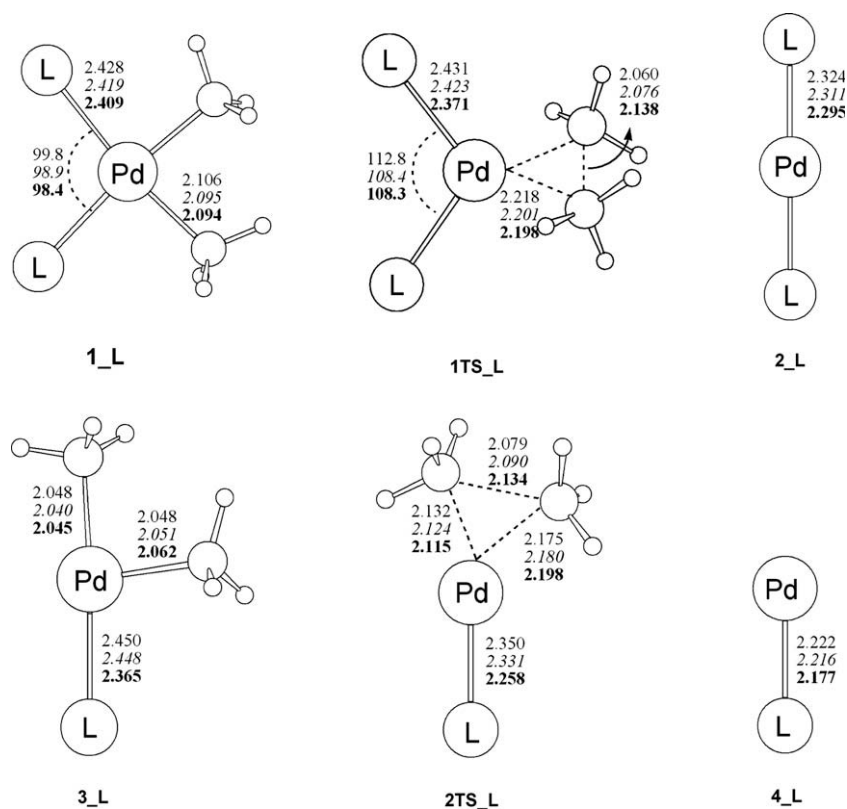

Fig. 2. Calculated structures for species involved in the Me–Me reductive elimination from L_2PdMe_2 (L = PMe_3, PH_3, PCl_3). Selected bond distances and angles are given in angstroms and degree, respectively. Data for L = PMe_3 are in plain text, for L = PH_3 in italics and L = PCl_3 in bold.
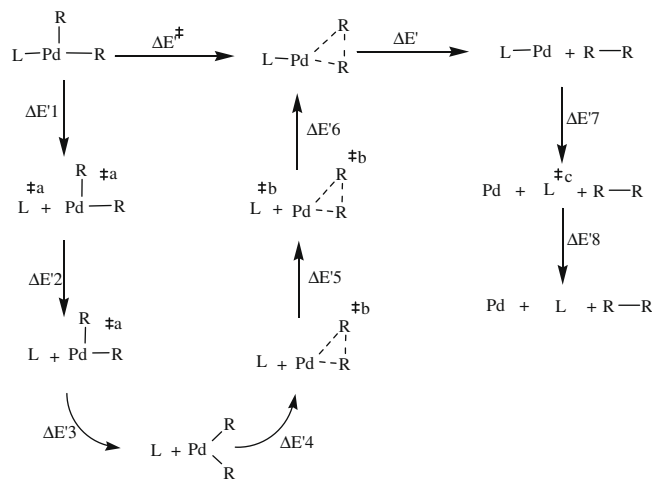
indicating an incorrect estimate of ΔG from the gas phase calculation. A precise estimate of ΔG in solution is too difficult to calculate. However, for the L-predissociation mechanism, one can obtain a rough estimate of the corresponding Gibbs free energy profile by deducting 8–10 kcal/mol from all the electronic energies given in the right-hand side of Fig. 1 relative to L_2PdMe_2. Thus, on the basis of this new correction, one can expect that the ethane reductive elimination from L_2PdMe_2 through the L-predissociation mechanism would be favored in solution over the direct mechanism, a result which agrees with experimental observations.

Structural parameters of **1_L**, **3_L**, **1TS_L**, and **2TS_L** are summarized in Fig. 2. For all the transition states **1TS_L**, a non-planar structure was located in which both the Pd–Me bonds are elongated and bent relative to the corresponding reactants. The ethane reductive elimination from the three coordinate $LPdMe_2$ species proceeding via transition states **2TS_L** involves migration of the methyl ligand trans to the vacant site toward the other methyl. In **2TS_L**, the bond distance between Pd and the migrating methyl ligand lengthens while the other Pd–Me bond distance remains fairly constant, though both the methyl ligands are bent to meet each other. From Figs. 1 and 2, one also can find a clear trend as follows: the more basic the phosphine ligand, the higher the activation barrier and the later the transition state.

To account for the trend in activation energy for the ethane elimination, an energy-decomposition analysis of reaction barriers using the BS1 basis set was carried out (Schemes 2 and 3) using the activation strain model [29] and the results of the analysis are summarized in Tables 1 and 2. Recalculation using the larger basis set and the geometries optimized by the B3LYP/BS2 calculations gives similar results to those listed in Tables 1 and 2 (see Tables S1 and S2 in Supplementary material) indicating the reliability of the standard BS1 basis set [30]. $\Delta E1$ ($\Delta E'1$) represents the energy required to dissociate L_2PdR_2 ($LPdR_2$) into fragments: $PdR_2^{\ddagger a}$ and $2L^{\ddagger a}$ ($L^{\ddagger a}$). $PdR_2^{\ddagger a}$ and $L^{\ddagger a}$ have the same geometry we found in the reactants. $\Delta E2$ and $\Delta E3$ ($\Delta E'2$ and $\Delta E'3$) involve relaxation of the $L^{\ddagger a}$ and $PdR_2^{\ddagger a}$ fragments into their equilibrium geometries. $\Delta E4$ and $\Delta E5$ ($\Delta E'4$ and $\Delta E'5$) refer to the energy needed to deform the phosphine and PdR_2 fragments to the geometries they acquire in the transition states. The interaction energy between the de-
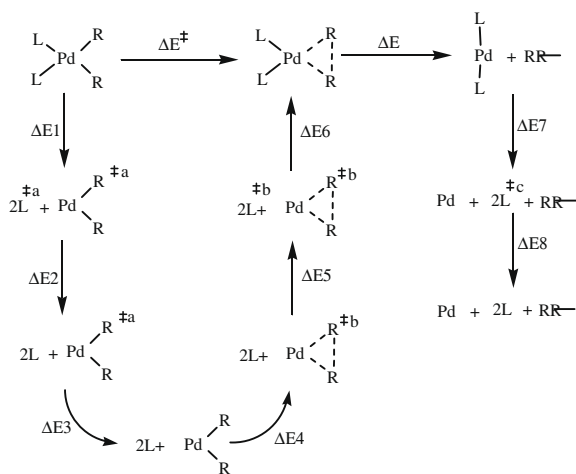
Scheme 2. $\Delta E1$ represents the energy required to dissociate L_2PdR_2 into fragments: $PdR_2^{\ddagger a}$ and $2L^{\ddagger a}$. $PdR_2^{\ddagger a}$ and $L^{\ddagger a}$ have the same geometry we found in the reactants. $\Delta E2$ and $\Delta E3$ involve relaxation of the $L^{\ddagger a}$ and $PdR_2^{\ddagger a}$ fragments into their equilibrium geometries. $\Delta E4$ and $\Delta E5$ refer to the energy needed to deform the phosphine and PdR_2 fragments to the geometries they acquire in the transition states. The interaction energy between the deformed $PdR_2^{\ddagger b}$ and $2L^{\ddagger b}$ fragments is represented by $\Delta E6$. $\Delta E7$ stands for the energy needed to separate PdL_2 into Pd and $2L^{\ddagger c}$. $\Delta E8$ is the energy released associated with the relaxation of $L^{\ddagger c}$ from the frozen geometry in PdL_2 to the optimized geometry (L).

Scheme 3. $\Delta E'1$ represents the energy required to dissociate $LPdR_2$ into fragments: $PdR_2^{\ddagger a}$ and $L^{\ddagger a}$. $PdR_2^{\ddagger a}$ and $L^{\ddagger a}$ have the same geometry we found in the reactants. $\Delta E'2$ and $\Delta E'3$ involve relaxation of the $L^{\ddagger a}$ and $PdR_2^{\ddagger a}$ fragments into their equilibrium geometries. $\Delta E'4$ and $\Delta E'5$ refer to the energy needed to deform the phosphine and PdR_2 fragments to the geometries they acquire in the transition states. The interaction energy between the deformed $PdR_2^{\ddagger b}$ and $L^{\ddagger b}$ fragments is represented by $\Delta E'6$. $\Delta E'7$ stands for the energy needed to separate PdL_2 into Pd and $L^{\ddagger c}$. $\Delta E'8$ is the energy released associated with the relaxation of $L^{\ddagger c}$ from the frozen geometry in PdL_2 to the optimized geometry (L).

formed $PdR_2^{\ddagger b}$ and $2L^{\ddagger b}$ ($L^{\ddagger b}$) fragments is represented by $\Delta E6$ ($\Delta E'6$). $\Delta E7$ ($\Delta E'7$) stands for the energy needed to separate PdL_2 (PdL) into Pd and $2L^{\ddagger c}$ ($L^{\ddagger c}$). $\Delta E8$ ($\Delta E'8$) is the energy released associated with the relaxation of $L^{\ddagger c}$ from the frozen geometry in PdL_2 to the optimized geometry (L).

From Table 1, one can find that upon going from L = PMe_3 to PCl_3, the sum of $\Delta E2$, $\Delta E3$, $\Delta E4$, and $\Delta E5$ remains nearly unchanged and could not thus be responsible for the differences in the activation energies. Both $\Delta E1$ and $\Delta E7$ increase from L = PCl_3 to PMe_3 and change significantly within a relatively wide range, implying that the phosphine-to-Pd σ-donation is dominating the bonding mode regardless of the nature of the oxidation sate of Pd. Unexpectedly, the same trend is not observed for $\Delta E6$. The interaction energy between the deformed PdR_2 and L fragments, $\Delta E6$, becomes less negative from L = PCl_3 to PH_3 and then becomes more negative from X = PH_3 to PMe_3. Also, it is of interest to note

Table 1
The energy-decomposition data (kcal/mol) using B3LYP/BS1 for the **1_L → 1TS_L → 2_L** + Me–Me conversion, where L = PMe_3, PH_3, and PCl_3, based on the illustration given in Scheme 2. The full energy-decomposition analyses are given in Supplementary material.

L	$\Delta E1$	$\Delta E6$	$\Delta E7$	$\Delta E8$	$\Delta E1 + \Delta E6$	$\Delta E2 + \Delta E3 + \Delta E4 + \Delta E5$
PMe_3	46.6	−38.0	72.0	−0.7	8.6	19.7
PH_3	34.3	−31.2	61.4	−0.7	3.1	20.3
PCl_3	28.7	−35.3	56.3	−0.2	−6.6	19.9

Table 2
The energy-decomposition data (kcal/mol) using B3LYP/BS1 for the **3_L → 2TS_L → 4_L** + Me–Me conversion, where L = PMe_3, PH_3, and PCl_3, based on the illustration given in Scheme 3. The full energy-decomposition analyses are given in Supplementary material.

L	$\Delta E'1$	$\Delta E'6$	$\Delta E'7$	$\Delta E'8$	$\Delta E'1 + \Delta E'6$	$\Delta E'2 + \Delta E'3 + \Delta E'4 + \Delta E'5$
PMe_3	23.5	−33.3	40.6	−0.4	−9.8	22.3
PH_3	16.7	−27.2	34.3	−0.3	−10.5	22.4
PCl_3	15.1	−27.0	36.2	−0.2	−11.9	22.3

that, in comparison with $\Delta E1$ and $\Delta E7$, the values of $\Delta E6$ span a relatively small range from -38.0 kcal/mol (L = PMe$_3$) to -31.2 kcal/mol (L = PH$_3$). The positive values of $\Delta E1 + \Delta E6$ for L = PMe$_3$ and PH$_3$ indicate that the coordination of the two phosphine ligands destabilizes the transition states **1TS_PMe$_3$** and **1TS_PH$_3$**. In other words, the Pd–L bonds, where L = PMe$_3$ and PH$_3$, become weaker upon going from **1_L** to **1TS_L**, as evidenced by the slight lengthening of the Pd–P bonds (Fig. 2). This makes the barrier to reductive elimination of ethane from L$_2$PdMe$_2$ relatively high. On the contrary, the coordination of the two PCl$_3$ ligands stabilizes transition state **1TS_PCl$_3$** (see the negative value of $\Delta E1 + \Delta E6$ for the PCl$_3$ case). Indeed, it is the much greater Pd–PCl$_3$ binding energy in **1TS_PCl$_3$** versus in **1_PCl$_3$** which makes the reaction barriers relatively small for (PCl$_3$)$_2$PdMe$_2$. The strongest Pd–L bonds are predicted for the products **2_L** which require the largest energies to dissociate PdL$_2$ to Pd and 2L (sum of $\Delta E7$ and $\Delta E8$ in Table 1). The Pd–L bond in **1_L** is weaker than in **2_L** because of the strong trans influence of the Me group.

The results of the energy-decomposition analysis for LPdMe$_2$ are listed in Table 2. Similar to what we found for the four coordinate species, the sum of $\Delta E'2$, $\Delta E'3$, $\Delta E'4$, and $\Delta E'5$ is nearly invariant to the modification of the ligand L and the Pd–L bond. The most dominant contribution to the difference in the reductive elimination barrier between the three and four coordinate species is the

change in the Pd–L bond strength. The negative value of $\Delta E'1 + \Delta E'6$ indicates that the Pd–L bonds become much stronger upon going from **3_L** to **2TS_L** (Table 2). The shorter Pd–L bond distance in **2TS_L** compared to in **3_L** further supports the claim here (Fig. 2). This result contrasts with the situation in the four coordinate species in which the Pd–L bonds, where L = PMe$_3$ and PH$_3$, are significantly weakened from **1_L** to **1TS_L**. The sum of $\Delta E'1$ and $\Delta E'6$ becomes slightly more negative from L = PMe$_3$ to PCl$_3$, indicating that the greatest strengthening of the Pd–L bonds is found for L = PCl$_3$. From these results, one may conclude that due to the much stronger Pd–L bond strength in **2TS_L** compared to in **3_L** the ethane reductive elimination occurs much more easily from the three coordinate species.

In the course of the activation reaction, two electrons are transferring into the empty d$_{x^2-y^2}$ orbital, as two Pd–R bonds are being broken and a new C–C bond is being formed. Analysis of our DFT wavefunctions confirms that (as suggested by Hoffman 30 years ago [11a]) the HOMO in **1TS_L** corresponds to the partially occupied d$_{x^2-y^2}$ orbital and has significant σ* antibonding character between the palladium metal center and the two L ligands (Fig. 3a). Thus, in general, the more basic the phosphine ligands, the stronger the Pd–L repulsive interaction, and the more destabilized the transition state relative to the reactant. In other words, the high instability of **1TS_PMe$_3$** relative to **1_PMe$_3$** could be mainly related
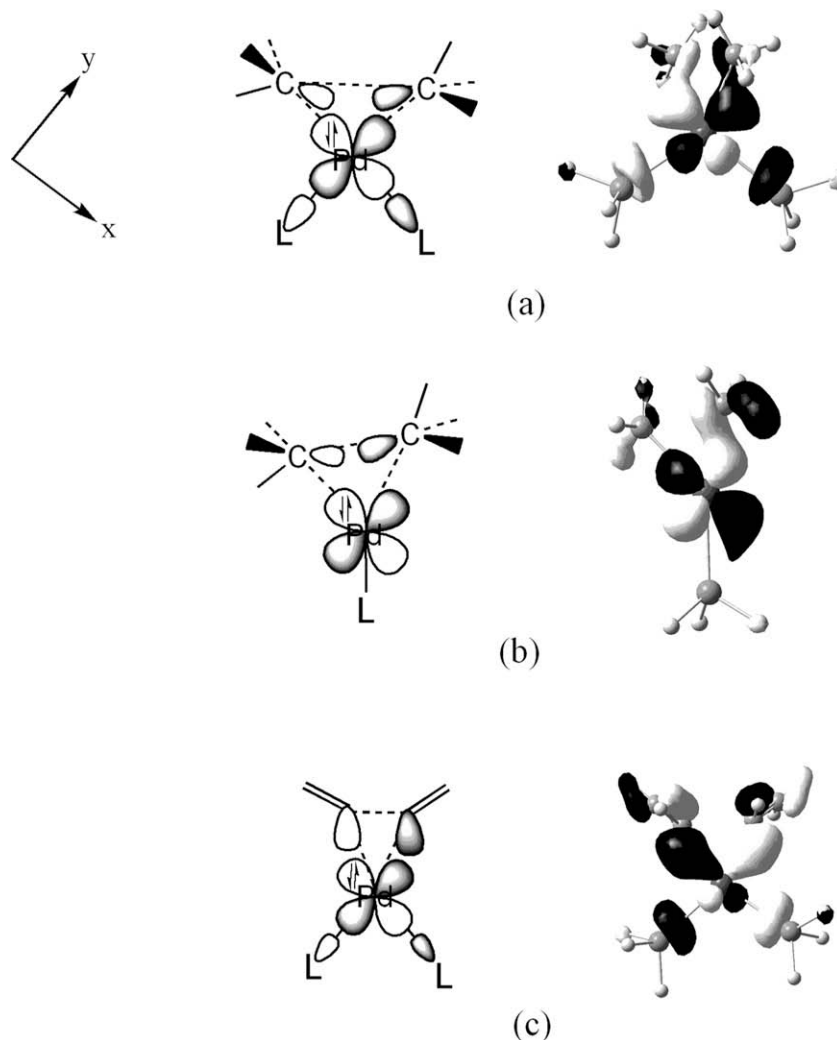

(a)

(b)

(c)

Fig. 3. The spatial plots and schematic illustrations showing how the partially occupied Pd d$_{x^2-y^2}$ orbital interacts with the coordinated ligands in (a) **1TS_L** and (b) **2TS_L** (c) **3TS_L**. In **1TS_L** and **2TS_L**, d$_{x^2-y^2}$ interacts with the Me$\cdots$Me σ* orbital while in **3TS_L**, it interacts with the vinyl$\cdots$vinyl σ*/π* hybrid orbital.

to the significantly greater repulsive interaction between PMe$_3$ and Pd. On the other hand, the occupied d$_{xy}$, d$_{xz}$, and d$_{yz}$ orbitals rise in energy with transferring the two electrons to the d$_{x^2-y^2}$ orbital. This process, which leads to an increase of electron density on the Pd metal center, facilitates the back-donation interaction from Pd to L. As expected, the PCl$_3$ ancillary ligands that are strong π-acceptor and weak σ-donor ligands stabilize the transition state much more than do the PMe$_3$ and PH$_3$ ligands. Thus, the low barrier for ethane elimination from L$_2$PdMe$_2$, where L is a weak donor and a strong acceptor ligand, can be rationalized as follows. First, the weakened bonding interaction between Pd and L in the transition state is less pronounced because the Pd–L repulsive interaction is not so strong. Second, the presence of the two strong π-accepting phosphine ligands seems to stabilize the occupied d$_π$ orbitals of the Pd metal center and consequently makes the reductive elimination transition state relatively more stable.

In contrast, the partially occupied d$_{x^2-y^2}$ orbital in **2TS_L** is non-bonding with respect to the ancillary ligand L and consequently affords no extra destabilization to the transition state (Fig. 3b). On the other hand, as discussed above, the negative values calculated for $\Delta E'1 + \Delta E'6$ suggest that the L ligand has a significant stabilizing effect on the transition state **2TS_L**. A plausible explanation for

the finding is as follows. Since the reductive elimination via **2TS_L** requires a drastic reorganization and change in the Pd–Me bonding, the tendency of the Me ligand trans to L to weaken the Pd–L bond decreases upon going from **3_L** to **2TS_L**. In other words, the trans influence of the Me ligands is far weaker in **2TS_L** than in **3_L**, resulting in the stronger bonding interaction between Pd and L in **2TS_L**. The Pd–L bond is shortened in **2TS_L** by 0.099–0.116 Å, reflecting the weaker trans influence of methyl in **2TS_L**. A combination of these two factors explains why **3_L** undergoes reductive elimination much more readily than **1_L**. From Fig. 1, one may also conclude that the phosphines with strong π-accepting ability are capable of stabilizing **2TS_PCl$_3$** more than **2TS_PH$_3$** and **2TS_PMe$_3$**, making the reductive elimination process kinetically more favorable.

3.2. Comparison of valence molecular orbitals of **1TS_PMe$_3$** and **2TS_PMe$_3$**

The main purpose of this subsection is to investigate how dissociation of one phosphine ligand affects the Pd d orbital energies in the transition states. The orbital diagrams drawn in Fig. 4 were obtained from a direct analysis of the DFT wavefunctions of
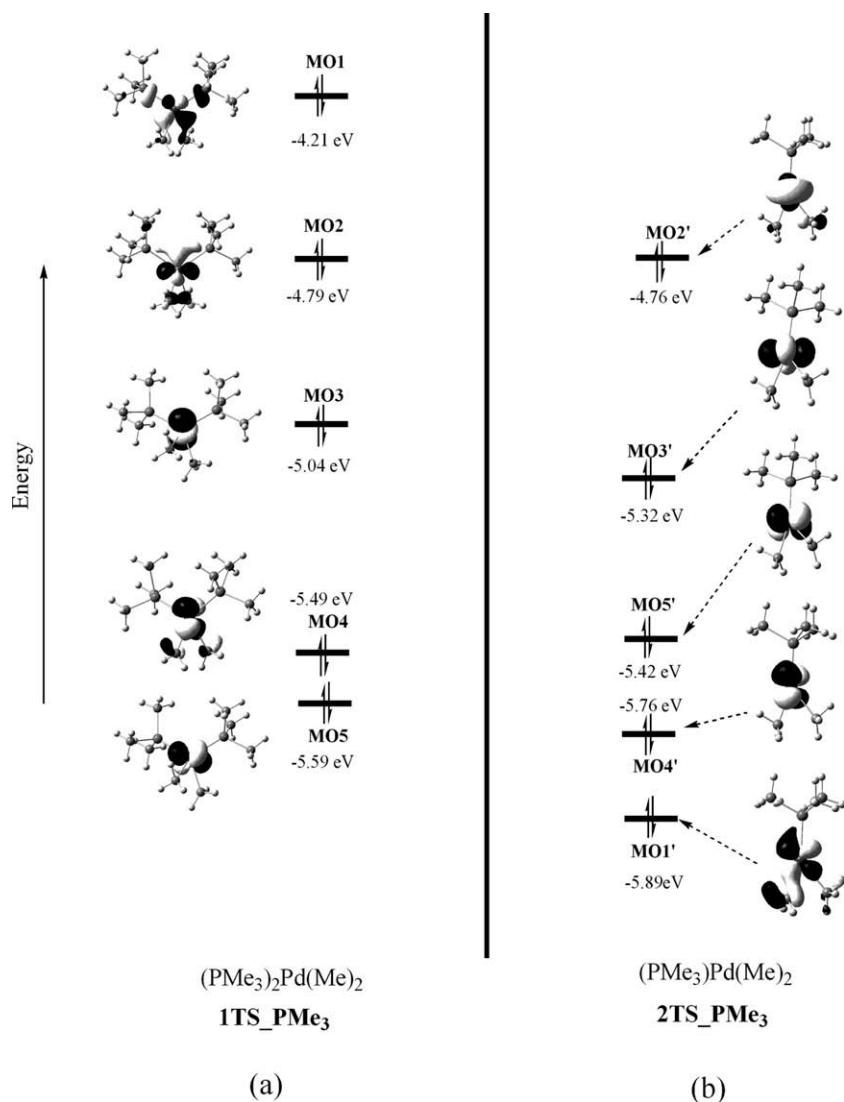

Fig. 4. Orbital diagrams showing the five highest occupied molecular orbitals for (a) **1TS_PMe$_3$** and (b) **2TS_PMe$_3$** along with their corresponding orbital energies.

1TS_PMe₃ and **2TS_PMe₃**. A similar trend was also observed for other complexes. These diagrams show the key role of the $d_{x^2-y^2}$ orbital in raising the reaction barrier through destabilizing the transition states in the four coordinate complexes with strong σ donor ligands. The $d_{x^2-y^2}$ orbital of **1TS_PMe₃** (**MO1** in Fig. 4a) suffers from the antibonding interaction with the PMe₃ σ orbitals while the other d orbitals do not undergo such antibonding interaction. The dissociation of one PMe₃ from **1TS_PMe₃** leading to the formation of **2TS_PMe₃** turns off the $\sigma PMe_3 - d_{x^2-y^2}$ antibonding interaction, causing the $d_{x^2-y^2}$ orbital (**MO1**) to substantially drop in energy (Fig. 4b). The energy difference between **MO1** and **MO1′** increases as the σ donating ability of L increases (1.68, 1.24, and 0.55 eV for L = PMe₃, PH₃, PCl₃, respectively), indicating that the strong σ-donor ligands (L) destabilize **MO1** more significantly. We can also see from Fig. 4 that upon going from **1TS_PMe₃** to **2TS_PMe₃**, the energy changes for the other d orbitals are insignificant suggesting that these orbitals would not play a crucial role in lowering of the reductive elimination barrier from **3_PMe₃** when compared to that from **1_PMe₃**. As mentioned above, the phosphine-to-Pd donation is dominating the bonding mode regardless of the nature of the oxidation sate of Pd. Thus, in the four coordinate complexes when L is a strong σ-donor ligand, it is expected that there will be greater repulsive interaction in **MO1**, further weakening the Pd–L bond strength in **1TS_L**, leading to the greater destabilization of **1TS_L**. In contrast, in the three coordinate complexes, such a destabilizing interaction disappears, providing a situation in which the reductive elimination barrier becomes low and mainly independent of the electronic nature of L.

3.3. Vinyl–vinyl elimination from $L_2Pd(vinyl)_2$ (L = PMe₃, PH₃, PCl₃)

Although the loss of Me–Me vs. vinyl–vinyl by reductive elimination has been studied previously by Morokuma and co-workers [10], we present here a more detailed molecular orbital rationalization of the differences between these two elimination reactions. To investigate the dependence of the ease of R–R reductive elimination from L_2PdR_2 on the reacting moieties, calculations were performed on the reductive elimination reaction from the vinyl complexes $L_2Pd(vinyl)_2$, where L = PMe₃, PH₃, PCl₃. The energy profiles for the species based on the two mechanisms suggested in Scheme 1 are shown in Fig. 5. In analogy to the Me–Me reductive elimination reaction from L_2PdMe_2, the decreasing order of the activation barrier to the vinyl–vinyl elimination from L_2PdMe_2 is L = PMe₃ > PH₃ > PCl₃. Comparing the energy profiles given in Figs. 1 and 5, one can find that, in accordance with the earlier findings [10], the reductive elimination reaction from $L_2Pd(vinyl)_2$ is easier than from L_2PdMe_2. The $\Delta E2 + \Delta E3 + \Delta E4 + \Delta E5$ term for $L_2Pd(vinyl)_2$ is much smaller than that for L_2PdMe_2 (Tables 1 and 3). This fact can be rationalized by the significant stabilizing interaction between the Pd d_π orbital and the hybrid obtained from the mixing of vinyl···vinyl σ* and π* orbitals [31]. In contrast, in transition states **1TS_L**, due to the lack of the hybrid orbital, the interaction between the d_π orbital of Pd and the strongly directional sp³ hybrid orbitals of the Me ligands becomes poor, making the reductive elimination reaction very difficult (Fig. 3a and c).

It is also worth noting that the dependence of the activation barrier on L for $(vinyl)_2PdL_2$ is much less significant than for $(Me)_2PdL_2$. For $(vinyl)_2PdL_2$ in comparison with L_2PdMe_2, the $\Delta E1 + \Delta E6$ terms lie within a more narrow range (Tables 1 and 3) indicating that the destabilization/stabilization exerted by L in **3TS_L** is not significantly affected by the phosphine substituents. Again, this behaviour can be understood in terms of the orbitals schematically shown in Fig. 3. From Fig. 3c, we can see that, in transition states **3TS_L**, the hybrid orbitals of the vinyl ligands are able to stabilize the Pd d_π orbital through a metal-to-vinyl interaction, bringing it into HOMO−5. This interaction alleviates
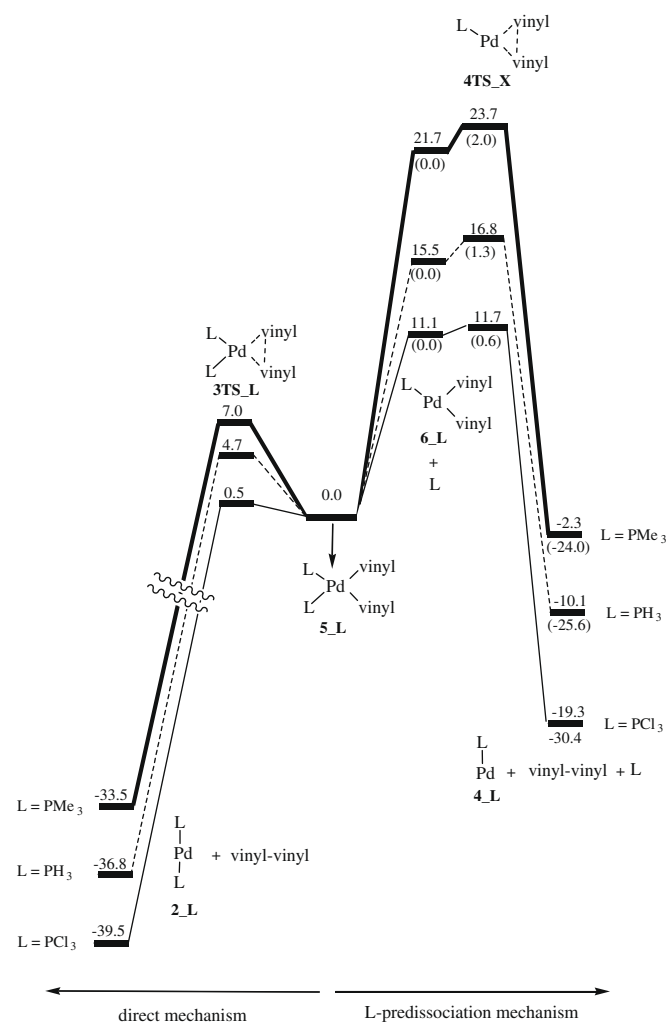

Fig. 5. Potential energy profiles calculated for the vinyl–vinyl reductive elimination from $(vinyl)_2PdL_2$ (L = PMe₃, PH₃, PCl₃) through both the direct and L-predissociation mechanisms using B3LYP/BS1. Values given in parentheses are relative to **6_L** + L. The electronic energies relative to the $(vinyl)_2PdL_2$ are given in kcal/mol.

Table 3
The energy-decomposition data (kcal/mol) using B3LYP/BS1 for the **5_L → 3TS_L → 2_L** + vinyl–vinyl conversion, where L = PMe₃, PH₃, and PCl₃, based on the illustration given in Scheme 2. The full energy-decomposition analyses are given in Supplementary material.

L	$\Delta E1$	$\Delta E6$	$\Delta E7$	$\Delta E8$	$\Delta E1 + \Delta E6$	$\Delta E2 + \Delta E3 + \Delta E4 + \Delta E5$
PMe₃	52.1	−47.7	72.0	−0.7	4.4	2.5
PH₃	36.7	−35.5	61.4	−0.7	1.2	3.5
PCl₃	28.5	−30.8	56.3	−0.2	−2.3	2.8

the Pd–L antibonding interactions in the transition state and decreases the donating capability of Pd to L, leading to the much smaller dependency of the elimination reaction on L. Evidence for this can be seen from the results of the NBO population analysis. For example, the change in the $d_{x^2-y^2}$ orbital population from **1_PMe₃** to **1TS_PMe₃** (0.401 e) is more significant than that from **5_PMe₃** to **3TS_PMe₃** (0.112 e). The trivial increase in the $d_{x^2-y^2}$ orbital population for **5_PMe₃ → 3TS_PMe₃** suggests that the Pd–L repulsive interaction in **3TS_PMe₃** should not be very severe.

Finally, it should be noted that, based on the calculated energy profile in Fig. 5, the vinyl–vinyl couplings through the direct mechanism are favored over the other mechanism even when the entro-

py contribution (8–10 kcal/mol) to the reaction is considered. This result is in agreement with the experimental studies that the C–C couplings involving unsaturated groups occur without prior phosphine dissociation.

3.4. Me–Me elimination from L_2PdMe_2 ($L = PPh_3$, PPh_2Me, $PPhMe_2$)

As mentioned in Section 1, for the rate of the R–R reductive elimination from L_2PdR_2 the following order was experimentally observed: $L = PPh_3 > PPh_2Me > PPhMe_2$. From the energy profile shown in Fig. 6, it is also obvious that the B3LYP calculations for L_2PdR_2 ($L = PPh_3$, PPh_2Me, $PPhMe_2$) also reproduce well the trends found from the experimental studies, regardless of the nature of reaction mechanism. Using ONIOM decomposition analysis, Ananikov et al. suggested that the steric effect of the L ancillary ligands promotes the R–R reductive elimination through the destabilization of the ground state, while the electronic effect of L influences the energy of the transition state [16]. These results raise a question concerning which effect dominates the reaction rate of the Me–Me elimination from L_2PdMe_2 ($L = PPh_3$, PPh_2Me, $PPhMe_2$). To address this question, the energy-decomposition analyses of the reaction barriers, shown in Schemes 2 and 3, were applied. Comparison of the data presented in Tables 4 and 5 provides the following conclusion. Each of the values of $\Delta E'1$, $\Delta E'7$, and $\Delta E7$ shows similarity

Table 4

The energy-decomposition data (kcal/mol) using B3LYP/BS1 for the $1\_L \rightarrow 1TS\_L \rightarrow 2\_L + Me$–Me conversion, where $L = PPh_3$, PPh_2Me, $PPhMe_2$ and PMe_3, based on the illustration given in Scheme 2. The full energy-decomposition analyses are given in Supplementary material.

L	$\Delta E1$	$\Delta E6$	$\Delta E7$	$\Delta E8$	$\Delta E1 + \Delta E6$	$\Delta E2 + \Delta E3 + \Delta E4 + \Delta E5$
PPh_3	39.3	−37.7	71.3	−0.6	1.6	18.9
PPh_2Me	43.8	−38.9	71.4	−1.0	5.0	19.8
$PPhMe_2$	46.9	−38.7	72.3	−0.6	8.2	19.7
PMe_3	46.6	−38.0	72.0	−0.7	8.6	19.7

Table 5

The energy-decomposition data (kcal/mol) using B3LYP/BS1 for the $3\_L \rightarrow 2TS\_L \rightarrow 4\_L + Me$–Me conversion, where $L = PPh_3$, PPh_2Me, $PPhMe_2$ and PMe_3, based on the illustration given in Scheme 3. The full energy-decomposition analyses are given in Supplementary material.

L	$\Delta E'1$	$\Delta E'6$	$\Delta E'7$	$\Delta E'8$	$\Delta E'1 + \Delta E'6$	$\Delta E'2 + \Delta E'3 + \Delta E'4 + \Delta E'5$
PPh_3	22.5	−32.2	39.7	−0.3	−9.7	22.4
PPh_2Me	22.4	−32.5	39.9	−0.4	−10.1	22.6
$PPhMe_2$	23.5	−33.2	40.5	−0.4	−9.7	22.3
PMe_3	23.5	−33.3	40.6	−0.4	−9.8	22.3

independent of the nature of the ancillary ligand L for the L_2PdMe_2 complexes, where $L = PPh_3$, PPh_2Me, $PPhMe_2$, PMe_3, suggesting that the electronic properties of all the phosphines should be comparable (Tables 4 and 5). The values calculated for $\Delta E2 + \Delta E3 + \Delta E4 + \Delta E5$ are fairly invariant to L, while the value for $\Delta E1 + \Delta E6$ becomes more positive as the size of L increases. $\Delta E1$ largely depends on the bulkiness of L while $\Delta E6$ does not. Indeed, the inclusion of two bulky L ligands results in the steric destabilization of the reactant, 1_L, as evidenced by the decreased value of $\Delta E1$ upon going from $L = PMe_3$ to PPh_3 (Table 4). Widening of the L–Pd–L bite angle and narrowing of the Me–Pd–Me angle in transition states $1TS\_L$ (Fig. 7) would vanish the steric effect introduced by the repulsive interaction between the L ligands and between the L and Me ligands, while the geometry change does not influence the electronic effect of L. The claim that the phosphine ligands PPh_3, PPh_2Me, $PPhMe_2$, and PMe_3 are electronically similar to one another can also find support from the result that the values of $\Delta E6$ for all the phosphines are nearly the same. This result suggests that the electronic effect of PR_3 is mainly reliant on the electronic nature of the substituents R. The reasons why the substituents R affect the electronic property of PR_3 has already been addressed by Frenking and co-workers [18]. Our detailed analysis confirms that the bulky phosphines such as PPh_3 and PPh_2Me facilitate the R–R reductive elimination mainly by destabilization of 1_L (Fig. 6) through steric rather than electronic means. The sterically larger phosphine ligands tend to reduce the energy required to dissociate one L from 1_L, subsequently lowering the Me–Me reductive elimination barrier through the L-predissociation mechanism. The comparable values calculated for $\Delta E'1$ suggest that the steric repulsion between the L and Me ligands is very small in the mono-phosphine systems. The above results also lead to the conclusion that, in calculations, the use of PMe_3 as a reliable model for PPh_3 would give accurate results provided that the steric effect introduced by the phosphines is insignificant.

For the sake of completeness, we also extended our calculations to the $(vinyl)_2Pd(PPh_3)_2$ system. Our calculations indicate that the barrier to the direct vinyl–vinyl elimination from $(vinyl)_2Pd(PPh_3)_2$ (2.1 kcal/mol) is approximately 4.9 kcal/mol smaller than from $(vinyl)_2Pd(PMe_3)_2$ (7.0 kcal/mol) indicating that, as expected, the steric repulsive interaction of the two PPh_3 ligands is also capable of promoting the vinyl–vinyl elimination process through the destabilization of 5_PPh_3.
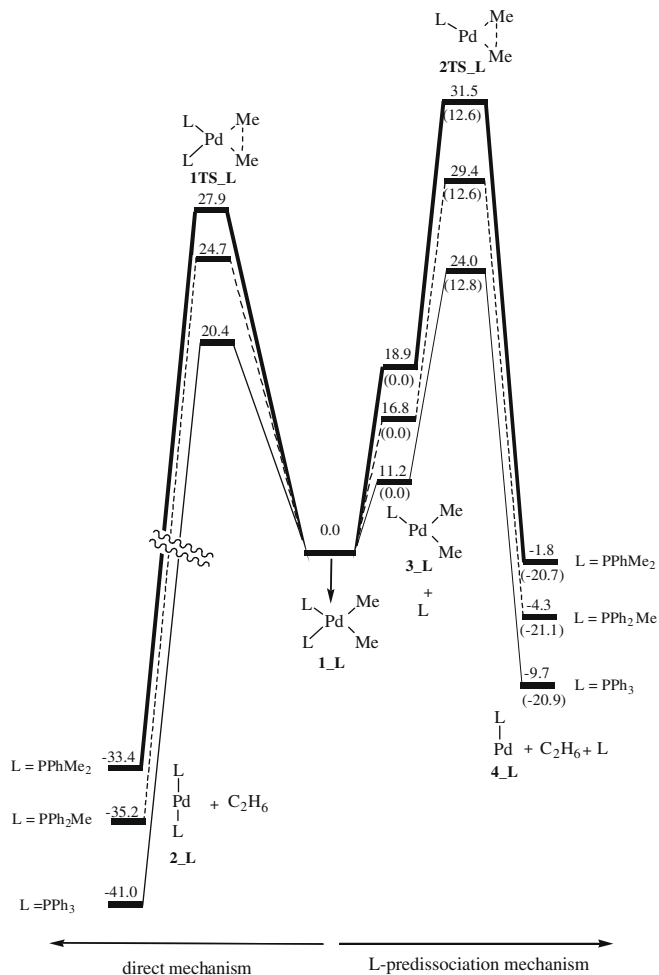

Fig. 6. Potential energy profiles calculated for the Me–Me reductive elimination from L_2PdMe_2 ($L = PPh_3$, PPh_2Me, $PPhMe_2$) through both the direct and L-predissociation mechanisms using B3LYP/BS1. Values given in parentheses are relative to $3\_L + L$. The electronic energies relative to the L_2PdMe_2 are given in kcal/mol.
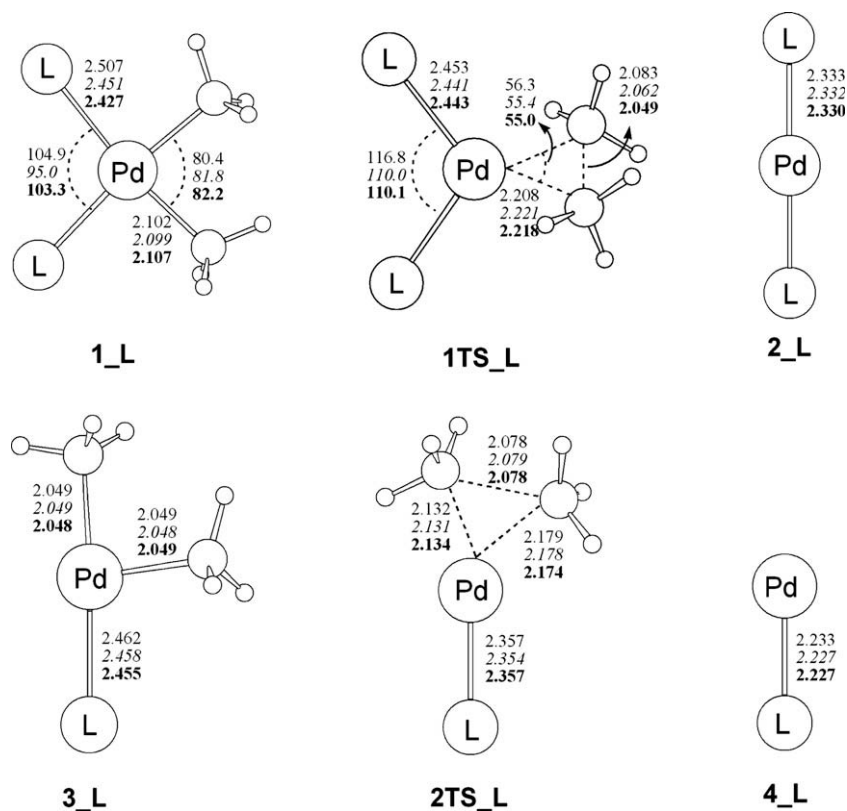
Fig. 7. Calculated structures for species involved in the Me–Me reductive elimination from L_2PdMe_2 (L = PPh_3, PPh_2Me, $PPhMe_2$). Selected bond distances and angles are given in angstroms and degree, respectively. Data for L = PPh_3 are in plain text, for L = PPh_2Me in italics and L = $PPhMe_2$ in bold.

4. Conclusions

This study has provided a detailed analysis of the steric and electronic effects of the ancillary ligands L in a series of reductive elimination reactions involving both model and real phosphine ligands. Electron donation from L plays an important role in reductive elimination from four coordinate L_2PdMe_2 but not from three coordinate $LPdMe_2$. In the former case the greater the electron donation or basicity of L, the greater the barrier and the later the transition state. This is because electron donation increases the σ^* antibonding between Pd and L in the transition structure. On the other hand, if L is a good π acceptor this stabilizes the occupied d_π orbital of Pd in the transition structure and lowers the barrier to reductive elimination. In the case of the elimination reactions involving three coordinate species $LPdMe_2$ as the intermediates, it is the dissociation of the first L ($L_2PdMe_2 \rightarrow LPdMe_2 + L$) which leads to the differences in the overall barrier and which is controlled by the basicity of L. Greater electron donation leads to greater L-to-Pd σ donation and a stronger Pd–L bond, and thus a greater overall barrier. A comparison of these results with the reductive elimination of 1,3-butadiene from divinyl palladium complexes L_2PdR_2 shows that the barriers are lower in the vinyl case because of a mix of orbital factors. Our results show that there is a significant stabilizing interaction between the Pd d_π orbital and the vinyl–vinyl hybrid σ^*/π^* orbitals in the reductive elimination transition structure. At the same time this Pd-R_2 orbital stabilization alleviates the potential antibonding interactions between Pd and L and makes the vinyl elimination much less susceptible to ancillary ligand effects. Energy-decomposition analyses have been used to elucidate the contributing factors to the activation energies for the reductive eliminations with the model phosphine ligands. These analyses have also been used to disentangle the electronic and steric effects involved in the larger ligand systems. The elec-

tronic effects of the experimentally reported ligands are found to be very similar to each other. On the other hand, steric effects lead to a destabilization of the reactant L_2PdMe_2 complexes but not the transition structures, which results in a decrease in the barriers to reductive elimination compared to the smaller phosphine ligands. These steric effects do not play a role in reductive elimination from $LPdMe_2$. These detailed analyses of the electronic and steric factors may be used to assist the design of systems which enhance or retard reductive elimination behaviour.

Appendix A. Supplementary material

Complete Ref. [19], Figs. S1–S4, Tables S1, S2, S5–S8 and tables giving Cartesian coordinates and electronic energies for all the calculated structures. Supplementary data associated with this article can be found, in the online version, at doi:10.1016/j.jorganchem.2009.02.011.

References

[1] (a) D. Milstein, J.K. Stille, J. Am. Chem. Soc. 100 (1978) 363;
　　(b) J.K. Stille, Angew. Chem., Int. Ed. Engl. 25 (1986) 508;
　　(c) P. Espinet, A.M. Echavarren, Angew. Chem., Int. Ed. 43 (2004) 4704.
[2] N. Miyaura, A. Suzuki, Chem. Rev. 95 (1995) 2457.

[3] T. Hiyama, in: F. Diederich, P.J. Stang (Eds.), Metal-Catalyzed Cross-Coupling Reactions, Wiley-VCH, Weinheim, 1998 (Chapter 10).

[4] (a) K. Sonogashira, J. Organomet. Chem. 653 (2002) 46;
(b) R.R. Tywinski, Angew. Chem., Int. Ed. 42 (2003) 1566.

[5] K. Tamao, K. Sumitani, M. Kumada, J. Am. Chem. Soc. 94 (1972) 4374.

[6] E. Negishi, L. Anastasia, Chem. Rev. 103 (2003) 1979.

[7] I.P. Beletskaya, A.V. Cheprakov, Chem. Rev. 100 (2000) 3009.

[8] (a) S. Niu, M.B. Hall, Chem. Rev. 100 (2000) 353;
(b) V.P. Ananikov, D.G. Musaev, K. Morokuma, J. Am. Chem. Soc. 124 (2002) 2839;
(c) D.S. McGuinness, B.F. Yates, K.J. Cavell, Organometallics 21 (2002) 5408;
(d) D.C. Graham, K.J. Cavell, B.F. Yates, Dalton Trans. (2005) 1093;
(e) E. Zuidema, P.W.N.M. van Leeuwen, C. Bo, Organometallics 24 (2005) 3703;
(f) D.C. Graham, K.J. Cavell, B.F. Yates, Dalton Trans. (2006) 1768.

[9] J.M. Brown, N.A. Cooley, Chem. Rev. 88 (1988) 1031.

[10] V.P. Ananikov, D.G. Musaev, K. Morokuma, Organometallics 24 (2005) 715.

[11] (a) K. Tatsumi, R. Hoffmann, A. Yamamoto, J.K. Stille, Bull. Chem. Soc. Jpn. 54 (1981) 1857;
(b) E. Negishi, T. Takahashi, K. Akiyoshi, J. Organomet. Chem. 334 (1987) 181;
(c) G. Mann, D. Baranano, J.F. Hartwig, A.L. Rheingold, I.A. Guzei, J. Am. Chem. Soc. 120 (1998) 9205;
(d) G. Mann, Q. Shelby, A.H. Roy, J.F. Hartwig, Organometallics 22 (2003) 2775.

[12] (a) F. Ozawa, T. Ito, Y. Nakamura, A. Yamamoto, Bull. Chem. Soc. Jpn. 54 (1981) 1868;
(b) F. Ozawa, K. Kurihara, T. Yamamob, A. Yamamoto, Bull. Chem. Soc. Jpn. 58 (1987) 399.

[13] (a) A. Gillie, J.K. Stille, J. Am. Chem. Soc. 102 (1980) 4933;
(b) M.K. Lou, J.K. Stille, J. Am. Chem. Soc. 103 (1981) 4174;
(c) A. Moravskiy, J.K. Stille, J. Am. Chem. Soc. 103 (1981) 4182.

[14] (a) S. Komiya, Y. Abe, A. Yamamoto, T. Yamamoto, Organometallics 2 (1983) 1466;
(b) S. Komiya, A. Shibue, Organometallics 4 (1985) 684;
(c) S. Komiya, S. Ozaki, A. Shibue, J. Chem. Soc., Chem. Commun. (1986) 1555;
(d) S. Komiya, A. Shibue, S. Ozaki, J. Organomet. Chem. 319 (1987) C31.

[15] (a) P.S. Braterman, R.J. Cross, G.B. Young, J. Chem. Soc., Chem. Commun. (1975) 627;
(b) P.S. Braterman, R.J. Cross, G.B. Young, J. Chem. Soc., Dalton Trans. (1976) 1310;
(c) P.S. Braterman, R.J. Cross, G.B. Young, J. Chem. Soc., Dalton Trans. (1976) 1306;
(d) P.S. Braterman, R.J. Cross, G.B. Young, J. Chem. Soc., Dalton Trans. (1977) 1892.

[16] S.A. Macgregor, G.W. Neave, C. Smith, Faraday Discuss. 124 (2003) 111.

[17] D. Choueiry, E.-I. Negishi, in: E. Negishi (Ed.), Handbook of Organopalladium Chemistry for Organic Synthesis, Wiley, New York, 2002.

[18] V.P. Ananikov, D.G. Musaev, K. Morokuma, Eur. J. Inorg. Chem. (2007) 5390.

[19] (a) K.L. Bartlett, K.I. Goldberg, T. Borden, J. Am. Chem. Soc. 122 (2000) 1456;
(b) K.L. Bartlett, K.I. Goldberg, T. Borden, Organometallics 20 (2001) 2669.

[20] (a) G. Frenking, K. Wichmann, N. Fröhlich, J. Grobe, W. Golla, D. Le Van, B. Krebs, M. Läge, Organometallics 21 (2002) 2921;
(b) D.S. Nemcsok, A. Kovács, V.M. Rayon, G. Frenking, Organometallics 21 (2002) 5803;
(c) A. Ariafard, J. Organomet. Chem. 689 (2004) 2275;
(d) R. Fazaeli, A. Ariafard, S. Jamshidi, E.S. Tabatabaie, K.A. Pishro, J. Organomet. Chem. 692 (2007) 3984.

[21] M.J. Frisch et al., GAUSSIAN 03, Revision B.05, GAUSSIAN, Inc., Pittsburgh, PA, 2003.

[22] (a) C.T. Lee, W.T. Yang, R.G. Parr, Phys. Rev. B 37 (1988) 785;
(b) A.D. Becke, J. Chem. Phys. 98 (1993) 5648;
(c) B. Miehlich, A. Savin, H. Stoll, H. Preuss, Chem. Phys. Lett. 157 (1989) 200.

[23] (a) P.J. Hay, W.R. Wadt, J. Chem. Phys. 82 (1985) 270;
(b) W.R. Wadt, P.J.J. Hay, Chem. Phys. 82 (1985) 284;
(c) P.J. Hay, W.R. Wadt, J. Chem. Phys. 82 (1985) 299.

[24] P.C. Hariharan, J.A. Pople, Theor. Chim. Acta 28 (1973) 213.

[25] A. Hgllwarth, M. Biihme, S. Dapprich, A.W. Ehlers, A. Gobbi, V. Jonas, F. Kijhler, R. Stegmann, A. Veldkamp, G. Frenking, Chem. Phys. Lett. 208 (1993) 237.

[26] E.D. Glendening, A.E. Read, J.E. Carpenter, F. Weinhold, NBO (Version 3.1), GAUSSIAN, Inc., Pittsburgh, PA, 2003.

[27] (a) H. Tamura, H. Yamasaki, H. Sato, S. Sakaki, J. Am. Chem. Soc. 125 (2003) 16114;
(b) M. Sumimoto, N. Iwane, T. Takahama, S. Sakaki, J. Am. Chem. Soc. 126 (2004) 10457;
(c) S. Sakaki, T. Takayama, M. Sumimoto, M. Sugimoto, J. Am. Chem. Soc. 126 (2004) 3332;
(d) A.A.C. Braga, G. Ujaque, F. Maseras, Organometallics 25 (2006) 3647.

[28] (a) E. Kelly, M. Seth, T. Ziegler, J. Phys. Chem. A 108 (2004) 2167;
(b) T. Ziegler, K. Vanka, Z.C.R. Xu, Chimie 8 (2005) 1552;
(c) S.-Y. Yang, M.J. Szabo, A. Michalak, T. Weiss, W.E. Piers, R.F. Jordan, T. Ziegler, Organometallics 24 (2005) 1242.

[29] (a) T. Ziegler, A. Rauk, Theor. Chim. Acta 46 (1977) 1;
(b) F.M. Bickelhaupt, J. Comput. Chem. 20 (1999) 114;
(c) A. Diefenbach, F.M. Bickelhaupt, J. Phys. Chem. A 108 (2004) 8640;
(d) A. Diefenbach, G.T. de Jong, F.M. Bickelhaupt, J. Chem. Theor. Comput. 1 (2005) 286.

[30] In a study like this on interaction and binding energies, basis set super position error (BSSE) could be an issue. To alleviate this concern we have recalculated the energy decomposition data given in Tables 1 and 2 using larger basis sets. These results are listed in Tables S1 and S2 in Supplementary material. These results show little changes and imply that the standard basis set (BS1) is reliable enough to be used for the energy decomposition analysis.

[31] A. Ariafard, Z. Lin, Organometallics 25 (2006) 4030.